Unizik Journal of Chemical & Environmental Engineering

https://journals.unizik.edu.ng/ujcee

Volume 1, Issue 1, Pages 084-096, 2026

Received: 23.05.2026
Accepted: 15.07.2026
Published: 25.07.2026

Biomass-Dependent Structural Evolution and Functionalization of Lignin under Peracetic Oxidation

Henry E. Oko [1,*], **Chigozie F. Uzoh** [1,2,3], **Loveth N. Emembolu** [1] **Lawrence I. Igbonekwu** [2]

[1] Department of Chemical Engineering, Nnamdi Azikiwe University, Awka Nigeria.
[2] Department of Petroleum Engineering, Nnamdi Azikiwe University, Awka Nigeria.
[3] Institute of Solids Process Engineering and Particle Technology, Hamburg University of Technology, Denickestraße 15, Hamburg, 21073, Germany
[*] Corresponding author's email: henryoko56@gmail.com

Abstract

The feedstock-dependent heterogeneity of lignin remains a major limitation in its rational design for interfacial applications, particularly as renewable oilfield demulsifier precursors. Although organosolv extraction and oxidative modification of lignin are widely reported, systematic cross-biomass evaluation under identical oxidative conditions remains largely unexplored, limiting the ability to decouple intrinsic biomass effects from reaction-driven transformations and constraining predictive materials design. In this study, lignins were extracted from rice husk (RH), sawdust (SD), and empty palm bunch (EPB) via an organic-acid organosolv process and subsequently oxidized using in-situ generated peracetic acid to engineer surface polarity and functionality. Structural evolution was characterized using FTIR, SEM, EDX, and TGA. FTIR analysis revealed consistent enhancement of carbonyl stretching (around 1740–1715 cm^{-1}) following oxidation, confirming oxygen incorporation while preserving aromatic backbone integrity (~1600–1510 cm^{-1}). SEM demonstrated oxidation-induced disruption of supramolecular packing, producing fractured morphologies indicative of increased surface accessibility. EDX confirmed biomass-specific inorganic signatures, with RH lignin exhibiting pronounced silica retention, whereas SD and EPB contained comparatively lower mineral content. TGA profiles showed broad lignin degradation behavior, with residual mass strongly correlated to mineral burden. Importantly, oxidative structural reconfiguration was systematically governed by biomass origin, with SD lignin exhibiting the most pronounced functionalization, RH lignin showing mineral-induced heterogeneity, and EPB displaying intermediate transformation behavior. These findings establish biomass origin as a predictive design parameter in oxidative lignin engineering and provide mechanistic insight relevant to the future development of lignin-derived green materials for interfacial and surface-active applications.

Keywords: Lignin; organosolv; peracetic oxidation; rice husk; sawdust; empty palm bunch; structural evolution; biomass dependence

1. Introduction

The global transition toward sustainable process industries has intensified research into lignocellulosic biomass as a renewable platform for advanced materials and specialty chemicals. Among its structural components, lignin is the most abundant renewable aromatic polymer and represents the largest natural reservoir of phenolic carbon (Saadan et al., 2024; Ma et al., 2021). Despite this abundance, more than 90% of industrial lignin is currently combusted for low-value energy recovery rather than upgraded into functional materials (Agrawal et al., 2025). This limited utilization is primarily attributed to its structural heterogeneity, feedstock variability, and the absence of systematic structure–property understanding required for rational material design.

From a materials perspective, lignin possesses an inherently amphiphilic architecture composed of aromatic domains, aliphatic side chains, hydroxyl groups, and ether linkages. These features provide a versatile platform for engineering surface-active materials where polarity, intermolecular interactions, and thermal stability govern interfacial performance (Gusiatin & Pawłowski, 2016; Suota et al., 2021). In petroleum production systems, crude oil is frequently produced as stable water-in-oil emulsions due to naturally occurring surface-active species such as asphaltenes and resins. These emulsions increase viscosity, reduce separation efficiency, and elevate operational costs in upstream processing (Rashid et al., 2018). Chemical demulsifiers are therefore essential for destabilizing interfacial films and promoting phase separation. However, most commercial demulsifiers are petroleum-derived and environmentally persistent (Chotirotsukon et al., 2023). The development of renewable, structurally engineered lignin derivatives as potential demulsifier precursors aligns with sustainability goals and circular economy strategies. Although direct interfacial performance evaluation is beyond the scope of the present study, understanding biomass-governed structural evolution remains essential for rational future design of lignin-derived surface-active systems.

Organosolv extraction methods have been widely adopted to obtain relatively pure, sulfur-free lignin fractions with preserved functional groups suitable for downstream modification (Schramm, 1992; Kang et al., 2018). Oxidative treatments, particularly peracetic acid systems generated in situ from acetic acid and hydrogen peroxide, have been shown to introduce oxygenated functionalities while largely maintaining aromatic backbone integrity (Ragauskas et al., 2014; Zhao et al., 2009). Such modifications enhance polarity, hydrogen bonding capacity, and dipolar interactions, which are directly relevant to interfacial activity. However, most studies focus on lignin derived from a single biomass source or employ varying processing conditions, making it difficult to distinguish whether observed structural transformations arise from intrinsic biomass chemistry or from reaction conditions.

A critical but underexplored challenge in lignin materials engineering is the lack of controlled comparative studies that isolate feedstock effects under identical processing environments. Without such controlled evaluation, biomass-derived structural variability—including differences in syringyl/guaiacyl composition, crosslink density, and inorganic content—cannot be decoupled from oxidation chemistry. This limitation restricts the development of predictive structure–property relationships necessary for rational design of lignin-based materials for interfacial applications.

Rice husk (RH), sawdust (SD), and empty palm bunch (EPB) were selected in this study as representative agro-industrial residues with distinct compositional characteristics. Rice husk is particularly rich in silica, which can influence both structural heterogeneity and thermal behavior, while sawdust and oil-palm residues exhibit differing lignin architectures and mineral contents (Mesa et al., 2011). These feedstocks are widely available and underutilized, making them attractive candidates for scalable lignin valorization.

To address this gap, this study performs a controlled cross-biomass evaluation of lignin oxidation under identical peracetic acid conditions, enabling direct assessment of feedstock-governed structural evolution. By integrating FTIR, SEM, EDX, and TGA analyses, this work establishes explicit links between functional group transformation, morphological restructuring, inorganic inheritance, and thermal behavior. The central contribution is the identification of biomass origin as a governing design parameter in oxidative lignin engineering, providing

a comparative mechanistic framework relevant to future development of lignin-derived interfacial and surface-active materials. The contribution of this study can therefore be articulated as follows: (i) a controlled cross-biomass comparison of peracetic oxidation across three structurally distinct agro-waste lignins under identical processing conditions; (ii) integrated multi-instrument characterization linking functional group evolution, morphology, mineral inheritance, and thermal stability; (iii) explicit correlation between silica-rich biomass composition and residual thermal behavior; and (iv) establishment of biomass origin as a rational comparative parameter in oxidative lignin engineering. Beyond fundamental characterization, the findings provide mechanistic insight relevant to the future development of lignin-derived renewable demulsifier precursors, surface-active materials, and sustainable oilfield chemical systems derived from circular biomass resources.



Figure 1. Representative agro-industrial biomass feedstocks used in this study: rice husk (RH), sawdust (SD), and empty palm bunch (EPB).

2. Materials and Methods

2.1 Raw Materials Preparation

Rice husk (RH), sawdust (SD), and empty palm bunch (EPB) were collected from agro-industrial processing facilities located in Anambra State, Nigeria. The materials were washed thoroughly with distilled water to remove dust and adhering impurities, then oven-dried at 70 °C for 24 h until constant weight was achieved. The dried biomass was milled and sieved to obtain particle sizes below 500 μm to ensure uniform extraction efficiency.

2.2 Organosolv Extraction of Lignin

Lignin was extracted using an acetic acid-based organosolv process. For each biomass, 50 g of dried, milled material was mixed with 500 mL of 80% (v/v) aqueous acetic acid solution (solid-to-liquid ratio 1:10 w/v). The mixture was transferred into a round-bottom flask equipped with a reflux condenser and heated at 110 °C for 3 h under continuous magnetic stirring at 500 rpm.

After extraction, the hot slurry was filtered to separate the solid residue. The filtrate containing dissolved lignin was diluted with three volumes of cold distilled water to precipitate lignin. The precipitated lignin was allowed to settle for 12 h, followed by centrifugation at 4000 rpm for 10 min. The recovered lignin was washed repeatedly with distilled water until neutral pH was achieved and then oven-dried at 60 °C to constant weight.

The dried lignins were designated as:

- RH (Rice husk lignin)
- SD (Sawdust lignin)

- EPB (Empty palm bunch lignin)

2.3 Lignin Extraction Yield

Lignin yield was calculated using the following equation:

$$Lignin\ Yield\,(\%) = \frac{W_L}{W_B}(1)$$

Where:

W_L = mass of dried lignin recovered (g)

W_B = initial dry mass of biomass used (g)

Extraction efficiency was compared across the three biomass sources to evaluate feedstock-dependent solubilization behavior.

2.4 Peracetic Acid Oxidation

Peracetic acid was generated in situ by mixing glacial acetic acid and hydrogen peroxide (30 wt%) in a 4:1 volume ratio. The mixture was allowed to equilibrate at room temperature for 1 h to ensure formation of peracetic acid.

For oxidation, 10 g of dried lignin was dispersed in 200 mL of the prepared peracetic acid solution. The suspension was maintained at 80 °C for 2 h under continuous stirring. The reaction was conducted under atmospheric pressure.

After oxidation, the mixture was cooled and diluted with excess distilled water to quench residual oxidant. The oxidized lignin was recovered by filtration, washed thoroughly with distilled water until neutral pH, and oven-dried at 60 °C to constant weight.

The oxidized samples were designated:

- ORH (Oxidized rice husk lignin)
- OSD (Oxidized sawdust lignin)
- OEPB (Oxidized empty palm bunch lignin)

2.5 Oxidation Mass Recovery

Oxidation recovery was calculated as:

$$Mass\ Recovery\,(\%) = \frac{W_O}{W_R} x\,100 \qquad (2)$$

Where:

W_O = mass of oxidized lignin recovered (g)

W_R = mass of raw lignin subjected to oxidation (g)

This parameter was used to assess the extent of oxidative degradation versus controlled functionalization.

2.6 Fourier Transform Infrared Spectroscopy (FTIR)

FTIR spectra were recorded using a Thermo Scientific Nicolet iS10 FTIR spectrometer over the range of 4000–400 cm^{-1} at a spectral resolution of 4 cm^{-1} with 32 scans per sample. Samples were analyzed in the solid state using standard KBr pellet preparation techniques. Spectral interpretation focused on hydroxyl, carbonyl, aromatic skeletal, and ether-related vibrational bands to evaluate oxidative functionalization and structural evolution of the lignin samples.

2.7 Scanning Electron Microscopy (SEM)

Surface morphology was examined using a Phenom ProX scanning electron microscope equipped with integrated Energy Dispersive X-ray Spectroscopy (EDX) capability. SEM analysis was conducted at accelerating voltages between 10–20 kV. Samples were mounted on aluminum stubs using conductive carbon tape and sputter-coated with a thin layer of gold to minimize surface charging during imaging. Micrographs were obtained at different magnifications to evaluate particle aggregation, surface restructuring, and oxidation-induced morphological evolution.

2.8 Energy Dispersive X-ray Spectroscopy (EDX)

Elemental composition analysis was performed using the integrated EDX detector attached to the Phenom ProX SEM instrument. Spectra were acquired to determine the relative atomic percentages of major elements including carbon (C), oxygen (O), silicon (Si), potassium (K), and calcium (Ca). Data were collected from multiple scan regions for each sample to improve representativeness and minimize localized compositional bias.

2.9 Thermogravimetric Analysis (TGA)

Thermogravimetric analysis was performed using a PerkinElmer TGA 4000 thermogravimetric analyzer. Approximately 5–10 mg of each sample was heated from 30 °C to 600 °C at a constant heating rate of 5 °C min^{-1} under static air atmosphere. Weight-loss behavior, degradation temperatures, and residual mass were recorded to evaluate thermal stability and

oxidation-induced structural changes in the lignin samples.

3. Results and Discussion

The extraction yield and oxidation recovery values summarized in Table 1 provide quantitative insight into the biomass-dependent behavior of lignin during extraction and subsequent oxidative modification. Variations in yield reflect differences in structural composition and solubilization efficiency, while oxidation recovery indicates the extent of controlled functionalization relative to mass loss. These quantitative parameters establish a foundation for interpreting the structural, morphological, and thermal transformations discussed in subsequent sections.

The quantitative trends in Table 1 reveal clear feedstock-dependent differences. Sawdust (SD) exhibited the highest lignin yield and oxidation recovery, indicating greater structural accessibility and more uniform oxidative penetration. In contrast, rice husk (RH) showed comparatively lower recovery, which can be attributed to silica-associated structural constraints that limit homogeneous oxidation. Empty palm bunch (EPB) displayed intermediate behavior, consistent with its balanced compositional characteristics. These observations provide a quantitative basis for understanding the spectroscopic and morphological transformations discussed below.

Table 1. Lignin extraction yield and oxidation recovery for different biomass sources

Biomass Source	Lignin Yield (%)	Oxidation Recovery (%)	Interpretation
Rice husk (RH)	18.6 ± 0.5	84.2 ± 0.7	Moderate extraction; silica-associated structure limits uniform oxidation
Sawdust (SD)	21.3 ± 0.4	88.9 ± 0.6	Highest extraction efficiency and oxidation response due to low mineral interference
Empty palm bunch (EPB)	19.8 ± 0.6	86.5 ± 0.8	Intermediate behavior reflecting balanced structure and mineral content

3.1. FTIR spectroscopy: functional group evolution

The FTIR spectra (Figure 2), supported by the quantitative trends in Table 1 and the diagnostic assignments summarized in Table 2, reveal the characteristic structural fingerprints of lignin and clearly demonstrate oxidative modification.

A broad O–H stretching band around 3400–3500 cm^{-1} is observed in both raw and oxidized lignins, corresponding to phenolic and aliphatic hydroxyl groups engaged in hydrogen bonding. Following peracetic oxidation, moderate spectral redistribution within the hydroxyl stretching region was observed, particularly for RH-derived lignin, suggesting modification of hydrogen-bonding environments associated with oxidative functionalization. The effect was comparatively less pronounced for SD and EPB samples. (Suota et al., 2021; Rashid et al., 2018; Chotirotsukon et al., 2023).

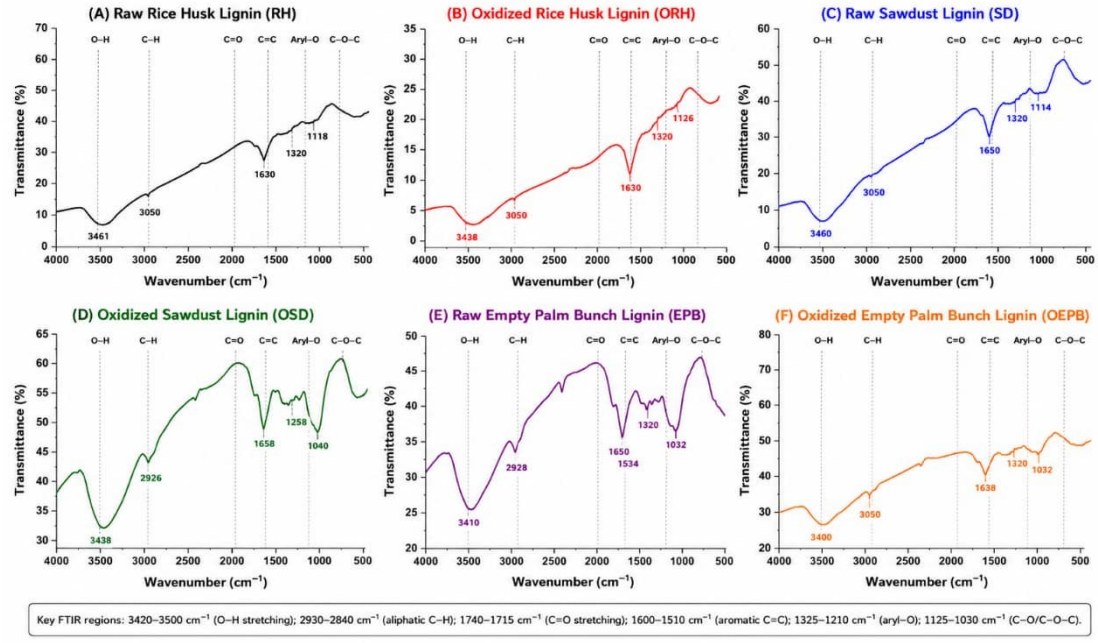


Figure 2. FTIR spectra of raw and oxidized lignin samples derived from rice husk (RH), sawdust (SD), and empty palm bunch (EPB).

Weak aliphatic C–H stretching features within the 2930–2840 cm^{-1} region remained partially observable after oxidation, suggesting relative preservation of the lignin aliphatic framework despite oxidative modification. Noticeable spectral evolution was observed within the carbonyl region around (~1740–1715 cm^{-1}) following oxidation, with oxidized samples exhibiting relatively stronger carbonyl-associated features consistent with incorporation of oxygenated functionalities during peracetic treatment. As summarized in Table 2, this band corresponds to unconjugated C=O stretching vibrations of ester, aldehyde, and carboxylic groups formed through oxidative modification of lignin side chains. The relative carbonyl enhancement observed for SD lignin compared with the other biomass-derived lignins suggests greater oxidative accessibility under the applied peracetic acid treatment conditions. This observation is consistent with its higher oxidation recovery (88.9 ± 0.6) as seen in (Table 1), indicating more effective functionalization.

Importantly, aromatic skeletal vibrations at ~1600 and 1510 cm^{-1} remain well defined across all oxidized samples (Figure 2), confirming that oxidation predominantly occurs at aliphatic side chains while preserving aromatic backbone integrity. This selective modification is critical for maintaining structural stability and amphiphilic balance in lignin-derived materials (Schramm, 1992; Kang et al., 2018; Ragauskas et al., 2014).

Bands in the 1325–1260 cm^{-1} region (aryl–O stretching of syringyl/guaiacyl units) and 1215–1030 cm^{-1} region (C–O/C–O–C stretching) exhibit subtle shifts and intensity variations following oxidation. These changes indicate partial modification of β–O–4 ether linkages and redistribution of oxygenated functional groups, consistent with controlled oxidative rearrangement rather than extensive depolymerization.

Clear biomass-dependent differences are evident. Sawdust (SD) lignin shows comparative enhancement in the carbonyl region, reflecting higher oxidative accessibility. Rice husk (RH) lignin exhibits broader spectral features and increased baseline complexity, particularly near ~1100 cm^{-1}, which is attributed to silica-associated matrices confirmed by EDX analysis (Section 3.3). Empty palm bunch (EPB) lignin displays intermediate behavior, with moderate carbonyl enhancement and relatively preserved spectral definition.

Overall, the FTIR analysis confirms that peracetic oxidation induces controlled structural functionalization across all lignins, with the extent and uniformity of transformation strongly governed by biomass origin. The combined interpretation of Table 1, Table 2, and Figure 2 demonstrates that oxidation proceeds primarily via side-chain modification while preserving aromatic backbone integrity, establishing the chemical basis for subsequent morphological and thermal evolution.

Table 2. Key FTIR bands used for structural interpretation.

Band (cm^{-1})	Assignment	Structural Interpretation
~3400–3500	O–H stretching (phenolic/aliphatic)	Hydrogen bonding and polarity; modified after oxidation
~2930–2850	Aliphatic C–H stretching	Side-chain preservation after oxidation
~1740–1715	C=O stretching (ester/carboxyl/ketone)	Oxidation marker; enhanced in ORH, OSD, OEPB
~1600–1510	Aromatic skeletal vibrations	Backbone retained across all samples
~1460–1425	Aromatic C–H deformation	Reflects packing and aromatic–aliphatic balance
~1265–1210	Aryl–O stretching (S/G units)	Sensitive to ether modification and bond rearrangement
~1125–1030	C–O / C–O–C stretching	Ether cleavage and oxygenated motif evolution

3.2. SEM morphology: oxidative surface restructuring

The SEM micrographs (Figure 3) reveal clear morphological transformation of lignin particles following peracetic oxidation. Raw lignins from all three biomass sources exhibit relatively compact, irregularly agglomerated structures with limited surface texturing. These agglomerates reflect strong intermolecular interactions and supramolecular packing arising from hydrogen bonding and π–π stacking between aromatic units. Such compact morphology is typical of precipitated organosolv lignin and has been reported for lignins recovered under mild acidic extraction conditions (Schramm, 1992; Mesa et al., 2011).

Following peracetic oxidation, all lignin samples exhibited measurable surface restructuring characterized by varying degrees of fracture development, surface roughening, and reduced agglomerate compactness. However, the extent and uniformity of restructuring differed significantly across biomass sources, reflecting feedstock-dependent oxidative accessibility and mineral-associated structural constraints. RH-derived lignin retained localized dense regions and heterogeneous fracture propagation patterns, likely influenced by silica-associated rigid domains. In contrast, SD lignin exhibited comparatively more uniform surface opening and fragmentation, consistent with reduced mineral interference and greater oxidative penetration. EPB samples displayed intermediate restructuring behavior.

This morphological transition indicates disruption of supramolecular packing and partial cleavage of ether-linked side chains, consistent with FTIR evidence of carbonyl enrichment. The development of micro-fractures and surface irregularities

suggests increased surface accessibility, which may enhance interfacial interaction potential in subsequent applications.

Biomass-specific distinctions are evident. Raw rice husk (RH) lignin exhibits the most heterogeneous morphology, with irregular domains and uneven surface features. Following oxidation (ORH), the surface becomes more fragmented yet retains localized dense regions. This heterogeneity is consistent with the mineral-associated matrix of rice husk, particularly silica domains confirmed by EDX analysis. The presence of inorganic inclusions likely influences fracture propagation and contributes to uneven surface restructuring.

Sawdust (SD) lignin demonstrates comparatively smoother agglomerates in the raw state, indicative of lower inorganic interference and more uniform lignin domains. Upon oxidation (OSD), SD lignin exhibits the most uniform and pronounced surface fracturing among the three feedstocks. The relatively homogeneous structural breakdown aligns with the stronger carbonyl amplification observed in FTIR, suggesting efficient oxidative penetration and side-chain modification.

Empty palm bunch (EPB) lignin presents intermediate behavior. Raw EPB lignin displays compact but less heterogeneous agglomerates than RH. After oxidation (OEPB), moderate surface opening and textural roughening are observed without extensive fragmentation. This balanced restructuring behavior is consistent with its intermediate oxygen incorporation and mineral composition profile.

Overall, SEM analysis confirms that peracetic oxidation induces measurable surface reconfiguration across all lignins. The extent and uniformity of morphological transformation are strongly influenced by biomass origin, with mineral-rich RH exhibiting heterogeneous fracture patterns, SD showing the most uniform restructuring, and EPB presenting intermediate characteristics. These observations complement FTIR findings and support the conclusion that oxidative structural engineering is feedstock-dependent.

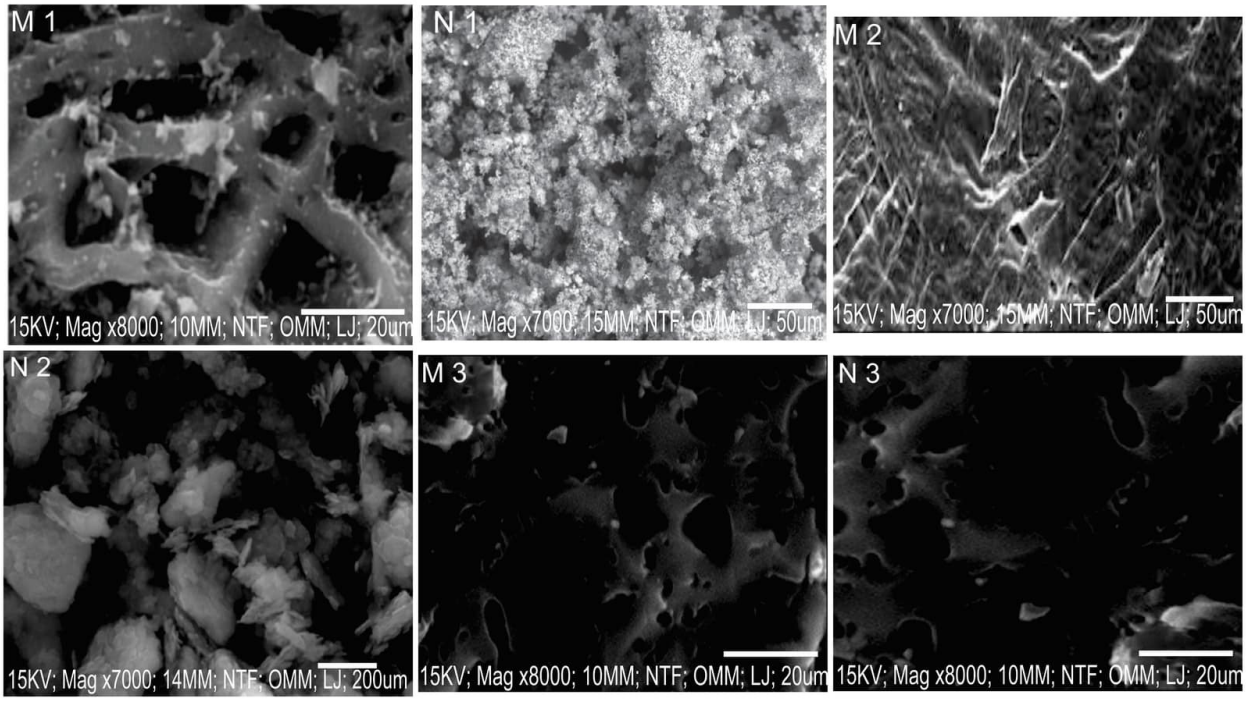


Figure 3: SEM combined panel (raw vs oxidized for RH, SD, EPB).

3.3 EDX spectroscopy: elemental composition and mineral inheritance

The EDX spectra (Figure 4) provide elemental confirmation of lignin composition and reveals biomass-dependent mineral signatures retained after organosolv extraction and oxidation. Carbon (C), oxygen (O), and silicon (Si) were identified as the principal detectable elements across the lignin samples, with RH-derived samples exhibiting particularly strong silicon contributions due to silica inheritance from rice husk biomass. Following oxidation, moderate oxygen enrichment trends were more distinguishable for SD and EPB samples, whereas RH-derived spectra remained strongly influenced by silica-associated elemental dominance.

Rice husk lignin (RH) exhibits a pronounced silicon (Si) signal in both raw and oxidized forms, confirming silica inheritance from the parent biomass. Rice husk is known to contain significant silica embedded within its structural matrix, and partial retention of this inorganic fraction during extraction is consistent with previous reports on silica-rich lignocellulosic residues (Calvo-Flores & Dobado, 2010; Vanholme et al., 2010). The persistence of silicon after oxidation indicates that the peracetic treatment predominantly modifies the organic fraction without dissolving or redistributing mineral components. This mineral presence explains the broader FTIR baseline near ~1100 cm^{-1} (Fig. 2) and the heterogeneous fracture patterns observed in SEM (Fig. 3).

sawdust (SD) lignin exhibits lesser silicon contribution than rice husk (RH) lignin and is characterized predominantly by carbon and oxygen signals, together with minor traces of potassium (K) and calcium (Ca), which are typical inorganic constituents of wood-derived biomass. The lower inorganic interference likely facilitates more uniform oxidative penetration, consistent with the stronger carbonyl enhancement and uniform surface restructuring observed for OSD. The oxygen-to-carbon balance appears slightly shifted after oxidation, reflecting incorporation of oxygenated functional groups.

Empty palm bunch (EPB) lignin displays intermediate elemental characteristics. Silicon levels are lower than in RH but trace inorganic elements such as K and Ca are detectable, reflecting mineral contributions from oil palm biomass. Oxidized EPB lignin shows modest oxygen enrichment relative to its raw counterpart, consistent with moderate oxidative transformation. The strong silicon dominance observed in RH-derived samples is attributed to the inherently high silica content of rice husk biomass. During organosolv extraction, the organic lignin fraction is preferentially solubilized, whereas significant portions of silica-associated inorganic domains remain structurally retained. As a result, residual silica persists after oxidation and contributes strongly to the EDX response and residual thermal behavior.

The integrated elemental interpretation is summarized in Table 3.

Table 3. Major elemental composition trends from EDX analysis.

Biomass	Dominant Elements	Oxygen Change After Oxidation	Silicon Presence	Mineral Influence
RH	C, O, Si	Moderate increase	High	Strong mineral inheritance
SD	C, O, Si (trace K, Ca)	Noticeable increase	Low (relative to RH)	Comparatively lower mineral contribution
EPB	C, O, Si (trace K, Ca)	Moderate increase	Moderate (relative to RH)	Intermediate mineral contribution

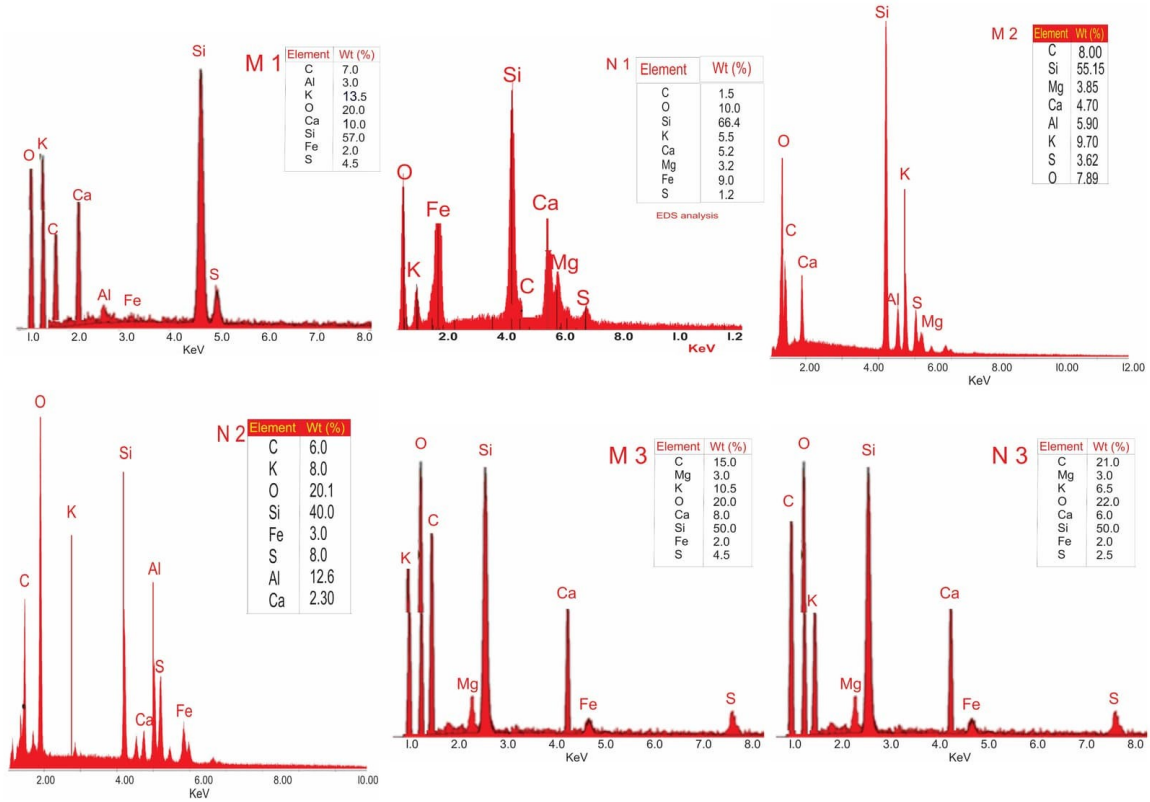


Figure 4: EDX combined panel (raw vs oxidized for RH, SD, EPB)

Overall, EDX analysis confirms that oxidative modification primarily affects the organic lignin fraction while preserving biomass-specific mineral signatures. The strong silicon inheritance in RH contributes to its heterogeneous morphology and higher thermal residue (Fig. 5), whereas the lower inorganic content of SD supports more uniform structural transformation. EPB maintains intermediate characteristics across elemental, morphological, and functional dimensions. These findings reinforce the concept that biomass origin governs not only chemical functionality but also inorganic inheritance and its downstream structural consequences.

3.4. Thermogravimetric analysis: thermal stability and oxidative restructuring

The TGA profiles (Figure 5) exhibit a dominant single major degradation stage for all lignin samples, occurring primarily between approximately 280–380 °C. A minor weight loss below ~100 °C corresponds to evaporation of physically adsorbed moisture and trace volatiles. Beyond this region, the samples remain thermally stable until rapid mass loss associated with lignin backbone depolymerization.

The principal degradation event is attributed to cleavage of β–O–4 ether linkages and scission of aliphatic side chains, processes characteristic of organosolv lignin systems (Kalapathy et al., 2000; Li et al., 2015). The relatively sharp single-step behavior observed across all samples suggests that extraction yielded comparatively homogeneous lignin fractions with limited polysaccharide contamination. This thermal pattern aligns with the preserved aromatic skeletal vibrations identified in FTIR.

Peracetic oxidation induces controlled but measurable shifts in degradation behavior. Oxidized samples generally show slight reductions in degradation temperature compared to their raw counterparts, indicating that incorporation of oxygenated groups weakens certain side-chain linkages. This observation is consistent with the enhanced carbonyl bands detected in FTIR (Figure 2), as introduction of ester/carboxyl functionalities can reduce bond dissociation energy in adjacent structures. Importantly, the major degradation still occurs above ~300 °C in most cases, confirming

preservation of aromatic backbone integrity despite oxidative modification.

Clear biomass-dependent distinctions are evident. Rice husk (RH) lignin exhibits comparatively higher residual mass at elevated temperatures (~5–7%), attributable to silica inheritance confirmed by EDX (Table 3). The inorganic fraction remains thermally stable and contributes directly to char formation. Sawdust (SD) lignin presents lower residual mass (~3–5%) and, in its oxidized form, slightly lower degradation temperature (~300–340 °C), suggesting greater oxidative accessibility and more extensive side-chain modification. Empty palm bunch (EPB) lignin demonstrates intermediate behavior, both in degradation temperature (~310–350 °C) and residual mass (~4–6%), consistent with its moderate mineral content and balanced functional transformation.

From a kinetic perspective, the dominant degradation stage reflects overlapping first-order depolymerization reactions governed primarily by ether bond cleavage and fragmentation of oxidized side chains. The modest reduction in degradation onset following oxidation suggests a slight decrease in apparent activation energy for thermal scission, while the persistence of significant char yield—particularly in RH—indicates aromatic condensation and mineral-assisted stabilization during carbonization.

Overall, TGA confirms that oxidative functionalization modifies lignin thermal response in a controlled and biomass-dependent manner. The degradation shifts correlate with carbonyl enrichment observed in FTIR, while residual behavior aligns directly with mineral signatures identified by EDX. These integrated observations reinforce that feedstock origin governs not only chemical reactivity but also downstream thermal behavior, providing a coherent structure–property framework for oxidative lignin engineering.

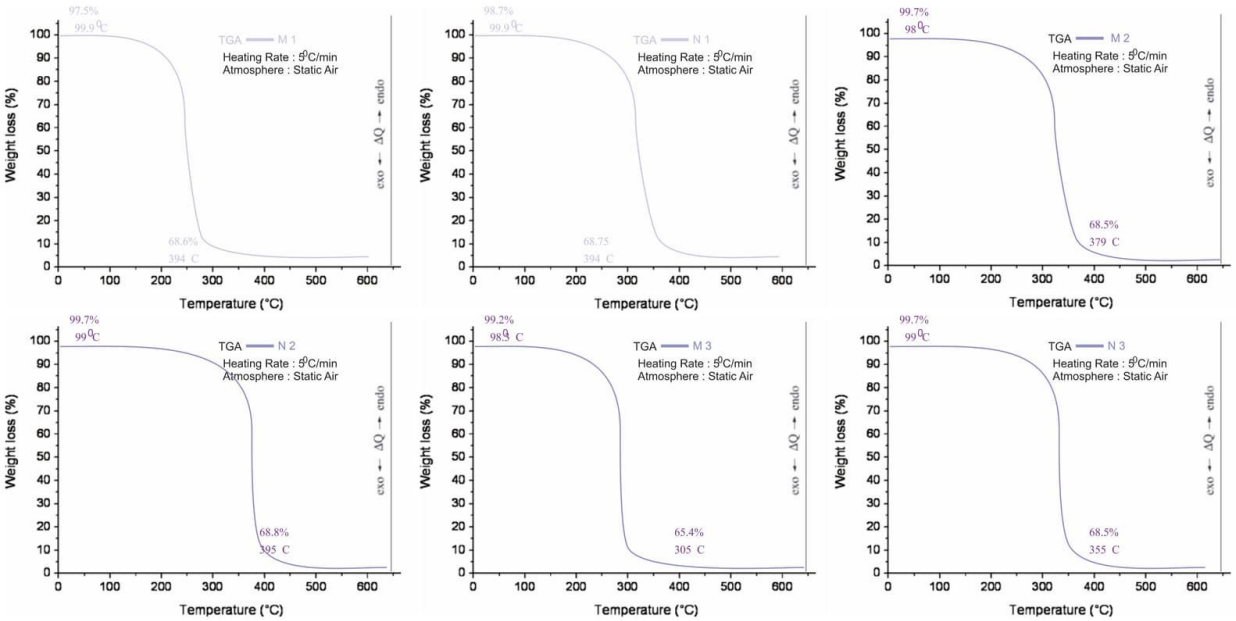


Figure 5: TGA combined panel (raw vs oxidized for RH, SD, EPB).

3.5. Integrated structure–property correlation and biomass-dependent oxidative response

The combined interpretation of FTIR, SEM, EDX, and TGA reveals a coherent biomass-dependent oxidative response across the three lignin feedstocks. While peracetic oxidation consistently introduces oxygenated functionalities into all lignins, the extent, manifestation, and structural consequences of this modification are intrinsically governed by biomass origin.

FTIR analysis demonstrates that oxidation proceeds primarily via side-chain functionalization, as evidenced by enhanced carbonyl bands (~1740–1715 cm^{-1}) with preserved aromatic skeletal vibrations (~1600–1510 cm^{-1}). This selective modification is reflected morphologically in SEM,

where disruption of supramolecular packing and surface fracturing accompany oxygen incorporation. The degree of restructuring correlates with oxidative accessibility: sawdust lignin shows the strongest relative carbonyl enhancement and most uniform surface fracture, while rice husk lignin exhibits heterogeneous restructuring influenced by inorganic domains. Empty palm bunch lignin consistently displays intermediate behavior across both functional and morphological dimensions.

EDX analysis provides the inorganic context for these structural differences. The pronounced silicon signature in rice husk lignin explains its heterogeneous morphology and higher thermal residue, confirming that mineral inheritance directly influences both surface evolution and carbonization behavior. In contrast, the lower inorganic content of sawdust lignin enables more homogeneous oxidative penetration, consistent with its stronger functional transformation and slightly reduced thermal stability after oxidation. EPB lignin, containing moderate mineral contributions, maintains intermediate characteristics across elemental, structural, and thermal metrics.

Thermogravimetric analysis further integrates these observations. Slight reductions in degradation temperature after oxidation align with carbonyl formation detected in FTIR, suggesting modest weakening of side-chain linkages. Meanwhile, residual mass trends correspond directly with mineral content identified by EDX, particularly in silica-rich RH samples. The persistence of degradation above ~300 °C across all oxidized samples confirms that aromatic backbone integrity remains largely intact despite oxidative restructuring.

Collectively, the data demonstrate that peracetic oxidation does not produce uniform structural evolution across lignins; rather, oxidative response is modulated by feedstock-specific architecture and mineral inheritance. Biomass origin therefore functions as a governing parameter in oxidative lignin engineering, influencing oxygen incorporation efficiency, surface accessibility, and thermal behavior in a coordinated manner. This integrated structural framework establishes a rational basis for feedstock selection in downstream lignin valorization strategies.

Conclusions

This study presents a controlled comparative structural evaluation of rice husk, sawdust, and empty palm bunch lignins under identical organosolv extraction and peracetic oxidation conditions. The results demonstrate that biomass origin governs oxidative functionalization, morphological restructuring, mineral retention, and thermal behavior. FTIR confirmed selective carbonyl enrichment, SEM revealed surface restructuring, EDX highlighted silica inheritance in RH, and TGA established biomass-dependent degradation profiles. These findings demonstrate that biomass origin significantly influences the structural, morphological, elemental, and thermal evolution of lignin during peracetic acid oxidation. The comparative analysis provides fundamental insight into biomass-dependent lignin functionalization and establishes a basis for future investigations into the development of lignin-derived functional materials. Although direct interfacial performance evaluation was beyond the scope of the present study. Future studies should therefore integrate interfacial characterization and demulsification performance evaluation to establish direct structure–performance relationships.

Funding

This manuscript received no funding

Acknowledgments

Not applicable

Conflicts of Interest

The authors declare no conflict of interest of any sort.

References

Agrawal, D., Tripathi, A., Pal, P., Hoque, M., Bharathi, S. D., & Samuel, J. (2025). Sustainable extraction strategy for lignin from coconut coir using organosolv and deep eutectic solvents (DES). *Waste and Biomass Valorization, 16*, 1599–1608. https://doi.org/10.1007/s12649-024-02758-z

Calvo-Flores, F. G., & Dobado, J. A. (2010). Lignin as renewable raw material. *ChemSusChem, 3*(10), 1227–1235.

Chotirotsukon, C., Jirachavala, K., Raita, M., Pongchaiphol, S., Hararak, B., Laosiripojana, N., & Champreda, V. (2023). Effects of thermal and physical modification on functional properties of organosolv lignin from sugarcane bagasse and its application in cosmeceutical products. *Frontiers in Chemical Engineering, 5*, Article 1099010. https://doi.org/10.3389/fceng.2023.1099010

Gusiatin, Z. M., & Pawłowski, A. (2016). Biomass for fuels—Classification and composition. In K. Bulkowska, Z. M. Gusiatin, E. Klimiuk, A. Pawłowski, & T. Pokój (Eds.), *Biomass for biofuels* (1st ed., Chapter 2). CRC Press.

Kalapathy, U., Proctor, A., & Shultz, J. (2000). A simple method for production of pure silica from rice hull ash. *Bioresource Technology, 73*(3), 257–262. https://doi.org/10.1016/S0960-8524(99)00127-3

Kang, W., Yin, X., Yang, H., Zhao, Y., Huang, Z., Hou, X., Sarsenbekuly, B., Zhu, Z., Wang, P., Zhang, X., Geng, J., & Aidarova, S. (2018). Demulsification performance, behavior and mechanism of different demulsifiers on the light crude oil emulsions. *Colloids and Surfaces A: Physicochemical and Engineering Aspects, 545*, 197–204. https://doi.org/10.1016/j.colsurfa.2018.02.055

Li, C., Zhao, X., Wang, A., Huber, G. W., & Zhang, T. (2015). Catalytic transformation of lignin for chemicals and fuels. *Chemical Reviews, 115*(21), 11559–11624. https://doi.org/10.1021/acs.chemrev.5b00155

Liu, W., & Budtova, T. (2013). Dissolution of lignin in ionic liquids and their application in lignin processing. *Green Chemistry, 15*(1), 226–234.

Ma, R., Sanyal, U., Olarte, M. V., Job, H. M., Swita, M. S., Jones, S. B., Meyer, P. A., Burton, S. D., Cort, J. R., Bowden, M. E., Chen, X., Wolcott,

M. P., & Zhang, X. (2021). Role of peracetic acid on the disruption of lignin packing structure and its consequence on lignin depolymerisation. *Green Chemistry, 23*(21), 8468–8479. https://doi.org/10.1039/D1GC02300D

Mesa, L., González, E., Cara, C., González, M., Castro, E., & Mussatto, S. I. (2011). The effect of organosolv pretreatment variables on enzymatic hydrolysis of sugarcane bagasse. *Chemical Engineering Journal, 168*(3), 1157–1162. https://doi.org/10.1016/j.cej.2011.02.003

Ragauskas, A. J., Beckham, G. T., Biddy, M. J., Chandra, R., Chen, F., Davis, M. F., Davison, B. H., Dixon, R. A., Gilna, P., Keller, M., Langan, P., Naskar, A. K., Saddler, J. N., Tschaplinski, T. J., Tuskan, G. A., & Wyman, C. E. (2014). Lignin valorization: Improving lignin processing in the biorefinery. *Science, 344*(6185), Article 1246843. https://doi.org/10.1126/science.1246843

Rashid, T., Gnanasundaram, N., Appusamy, A., Kait, C. F., & Thanabalan, M. (2018). Enhanced lignin extraction from different species of oil palm biomass: Kinetics and optimization of extraction conditions. *Industrial Crops and Products, 116*, 122–136. https://doi.org/10.1016/j.indcrop.2018.02.056

Saadan, R., Hachimi Alaoui, C., Ihammi, A., Chigr, M., & Fatimi, A. (2024). A brief overview of lignin extraction and isolation processes: From lignocellulosic biomass to added-value biomaterials. *Environmental Earth Sciences Proceedings, 31*(1), 3. https://doi.org/10.3390/eesp2024031003

Schramm, L. L. (Ed.). (1992). *Emulsions: Fundamentals and applications in the petroleum industry* (Advances in Chemistry Series, Vol. 231). American Chemical Society. https://doi.org/10.1021/ba-1992-0231

Suota, M. J., Kochepka, D. M., Ganter Moura, M. G., Pirich, C. L., Matos, M., Magalhães, W. L. E., & Ramos, L. P. (2021). Lignin functionalization strategies and the potential applications of its derivatives—A review. *BioResources, 16*(3), 6471–6511. https://doi.org/10.15376/biores.16.3.Suota

Vanholme, R., Demedts, B., Morreel, K., Ralph, J., & Boerjan, W. (2010). Lignin biosynthesis and structure. *Plant Physiology, 153*(3), 895–905. https://doi.org/10.1104/pp.110.155119

Zhao, X., Cheng, K., & Liu, D. (2009). Organosolv pretreatment of lignocellulosic biomass for enzymatic hydrolysis. *Applied Microbiology and Biotechnology, 82*(5), 815–827. https://doi.org/10.1007/s00253-009-1883-1

Title